The Action of Waving Cylindrical Rings in a Stokes Fluid

Journal:	*Journal of Fluid Mechanics*
Manuscript ID:	JFM-10-FT-0783
mss type:	Fast Track
Date Submitted by the Author:	12-Sep-2010
Complete List of Authors:	Nguyen, Hoa; Tulane University, Center for Computational Science Ortiz, Ricardo; Tulane University, Center for Computational Science Cortez, Ricardo; Tulane University, Mathematics Fauci, L.; Department of Mathematics, Tulane University
Keyword:	Micro-organism dynamics < Biological Fluid Dynamics, Swimming/flying < Biological Fluid Dynamics, Slender-body theory < Low-Reynolds-number flows

Under consideration for publication in J. Fluid Mech.

The Action of Waving Cylindrical Rings in a Stokes Fluid

HOA NGUYEN[1], RICARDO ORTIZ[1], RICARDO CORTEZ[1] AND LISA FAUCI[1]

[1]Department of Mathematics and Center for Computational Science,

Tulane University, New Orleans, LA 70118

(Received 11 September 2010)

Dinoflagellates are unicellular microorganisms that swim due to the action of two eucaryotic flagella: a trailing, longitudinal flagellum that propagates planar waves, and a transverse flagellum that propagates helical waves. Motivated by the wish to understand the role of the transverse flagellum in dinoflagellate motility, we study the fundamental fluid dynamics of a waving cylindrical tube wrapped into a closed helix. Given an imposed traveling wave on the structure, we determine that the helical ring propels itself in the direction normal to the plane of the circular axis of the helix. The magnitude of this translational velocity is proportional to the square of the helix amplitude. Additionally, the helical ring exhibits rotational motion tangential to its axis. These calculated swimming velocities are consistent when using instantaneous computations from the method of regularized Stokeslets, dynamic computations with regularized Stokeslets, and Lighthill's slender-body theory, except in cases when the slenderness parameter is not small. The translational velocity results are nearly indistinguishable using the three approaches, leading to the conjecture that the main contribution to this velocity at a cross-section is the far field flow generated by the portion on the opposite side of the ring. The largest contribution to the rotational velocity at a cross-section comes from

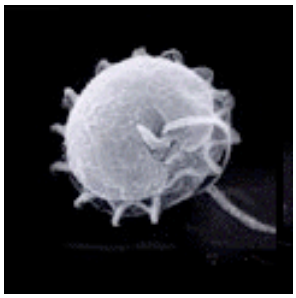

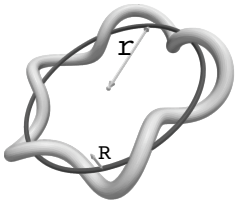

FIGURE 1. (left) A micrograph of the dinoflagellate *Pfisteria piscicida* (courtesy of the Aquatic Botany Lab, NC State). (right) A cylindrical ring that is helically-wrapped around a baseline circle of radius r. The amplitude of the helix is R.

the cross-section itself and others nearby, thus the geometric details of the slender body have a larger effect on the results.

---

1. Introduction

Dinoflagellates are unicellular microorganisms that are an important part of the aquatic food chain. Algal blooms of a certain dinoflagellate species give rise to "red tides" and bioluminescent dinoflagellates light up some marine bays (Latz *et al.* (2008)). Dinoflagellates swim due to the action of two eucaryotic flagella - a trailing, longitudinal flagellum that propagates planar waves, and a transverse flagellum that propagates helical waves (see Figure 1). The swimming trajectories of these cells are helical (Sheng *et al.* (2007)), and each cell exhibits both rotation about its longitudinal axis and translation along the same axis. The transverse flagellum wraps around the cell like a belt in a plane perpendicular to the trailing flagellum. An interesting aspect of the swimming motion of dinoflagellates is that there is no consensus in the literature about the principal roles of the two flagella. The transverse flagellum had been thought to be responsible for the cell's rotation, whereas the longitudinal flagellum was thought to induce forward motion of the cell (Cachon *et al.* (1991); Fenchel (2001); Gaines & Taylor (1985)). Fenchel (2001)

writes "In principle, the transversal flagellum should then only generate a net torque in a direction perpendicular to the longitudinal axis of the cell." However, it was observed that when some cells lacked a longitudinal flagellum, they still exhibited forward motion (Cachon *et al.* (1991)). More recently, Miyasaka *et al.* (2004) used resistive force theory to examine the functional role of the flagella of *Prorocentrum minimum*, and asserted that "The transverse flagellum works as a propelling device that provides the main driving force or thrust to move the cell along the longitudinal axis of its helical swimming path."

Motivated by the classical work in Taylor (1952) that examined the swimming of a waving cylindrical tail in a Stokes fluid, we isolate the function of the dinoflagellate transverse flagellum by addressing the simplified scenario of a helical tube wrapped into a closed ring. We ask the question: *If a traveling wave is imposed on the closed helical ring, what propulsion does it generate?* Our goal is to determine the fundamental fluid dynamics of a waving cylindrical ring in a Stokes fluid using various numerical approaches. For instantaneous fluid velocities generated by an imposed traveling wave on the structure, we use the slender-body theory in Lighthill (1976). Alternatively, we use the method of regularized Stokeslets (Cortez (2001); Cortez *et al.* (2005)) to compute the instantaneous swimming velocities. Our results show that the ring exhibits both rotational motion and translational progression in the direction perpendicular to the plane of the ring.

A dynamic model of the helical ring is also presented by constructing the elastic tube from nodes connected by springs whose forces are generated by time-varying resting lengths. The resting lengths as functions of time come from the idealized helical ring with a traveling wave passing through it. The nodes move with the fluid velocity at their locations, which is computed with the method of regularized Stokeslets. The simplified flagellum ring model is interesting on its own and sheds light on the mechanics of dinoflagellate motility, even if the model does not include all components of the organism.

The results also provide a test problem used to validate the use of regularized Stokeslets in the dynamic, elastic computations.

2. Mathematical Model

The idealized flagellum centerline is the closed circular helix described by:

$$\begin{cases} x(s,t) &= [r - R\sin(\frac{2\pi s}{\lambda} - \omega t)]\cos(\frac{s}{r}) \\ y(s,t) &= [r - R\sin(\frac{2\pi s}{\lambda} - \omega t)]\sin(\frac{s}{r}) \\ z(s,t) &= R\cos(\frac{2\pi s}{\lambda} - \omega t) \end{cases} \tag{2.1}$$

where $0 \leq s \leq 2\pi r = L$. The axis of this circular helix is a baseline circle of radius r in the plane $z = 0$. The helical amplitude is R, λ is wavelength, and $p = \frac{L}{\lambda}$ is the integral number of pitches around the ring. The surface of the helical ring is then formed by circular cross-sections of radius r_h placed normal to the above centerline. Figure 1 depicts the thick helical ring along with the baseline circle around which the ring is wrapped. As time t progresses, a wave with speed $w_s = \frac{\omega\lambda}{2\pi}$ is imposed to travel around the ring. Without the fluid, a point on the centerline would trace a circle of radius R. The temporal period of the wave is $T = \frac{2\pi}{\omega}$. Our goal is to determine how the imposed undulatory wave around the ring generates overall swimming of the ring in an unbounded, three-dimensional fluid.

We describe the fluid dynamics by the incompressible Stokes equations:

$$\mu\Delta\mathbf{u} = \nabla p + \mathbf{f} \tag{2.2}$$

$$\nabla \cdot \mathbf{u} = \mathbf{0} \tag{2.3}$$

Here, $\mathbf{u}$ is fluid velocity, p denotes pressure, and μ is dynamic viscosity. The force of the undulating ring on the surrounding fluid is given by $\mathbf{f}$. Note that when using slender

body theory (Lighthill (1976)), these forces are supported only along the one-dimensional centerline of the helical ring; however, when using regularized Stokeslets (Cortez (2001); Cortez *et al.* (2005)), the forces are distributed on the surface of the helical ring. In either case, the Stokes equations imply that the distribution of forces is linearly related to the distribution of velocities.

2.1. *Instantaneous fluid velocity computations*

In the static computations of instantaneous flows, we begin with an equation that encodes the linear relationship between the fluid velocity and the forces exerted by the flagellum. Generically,

$$\mathbf{u}(\mathbf{x}) = \mathcal{L}(\mathbf{x})[\mathbf{f}] \tag{2.4}$$

represents a slender-body theory, the regularized Stokeslet, or some other formulation. Assuming the velocity distribution on the helical ring implied by Eq. (2.1), we must compute $\mathbf{f}$. However, for steady state swimming of the ring, we ensure conservation of linear and angular momentum by imposing

$$\int_D \mathbf{f}(\mathbf{x}) ds(\mathbf{x}) = 0 \tag{2.5}$$

$$\text{and } \int_D \mathbf{x} \times \mathbf{f}(\mathbf{x}) ds(\mathbf{x}) = 0 \tag{2.6}$$

where D is the surface or filament supporting the force $\mathbf{f}$. The discretization of Eq. (2.4) with N points results in $3N$ equations for the $3N$ unknown force components. Eq. (2.5)-(2.6) represent six scalar constraints on the forces, which can be met by introducing six more degrees of freedom: an overall translational velocity $\mathbf{U}$ and overall rotational velocity $\mathbf{\Omega}$ of the ring.

2.1.1. *Slender body framework*

According to the theory in Lighthill (1976), Eq. (2.4) evaluated on the centerline is

$$8\pi\mu\mathbf{u}(\mathbf{x}(s_0)) = 2\mathbf{f}_n + \int_{r_0>h_0} \frac{\mathbf{f}(s)}{r_0} + \frac{(\mathbf{f}(s)\cdot\mathbf{r}_0)\mathbf{r}_0}{r_0^3} ds \tag{2.7}$$

where the helical ring centerline is given parametrically by $\mathbf{x}(s)$, $\mathbf{r}_0 = \mathbf{x}(s) - \mathbf{x}(s_0)$, $r_0 = \|\mathbf{r}_0\|$ and $\mathbf{f}_n = \mathbf{f} - (\mathbf{f}\cdot\tau)\tau$ ($\tau = \mathbf{x}'(s)/\|\mathbf{x}'(s)\|$ is the unit tangential vector). The integral is along the filament with the portion $[s_0 - h_0, s_0 + h_0]$ removed, where $h_0 = r_h\sqrt{e}/2$ with r_h equal to the helical tube radius.

2.1.2. *Regularized Stokeslet framework*

This formulation begins with the surface representation of the forces as

$$\mathbf{F}(\mathbf{x}) = \int_D \mathbf{f}(s)\phi_\epsilon(\mathbf{x} - \mathbf{x}(s))ds$$

where $\phi_\epsilon(\mathbf{x})$ is a *cutoff function* with the property that $\iiint \phi_\epsilon(\mathbf{x})d\mathbf{x} = 1$. Using the particular cutoff function in Cortez *et al.* (2005) leads to the following version of Eq. (2.4)

$$8\pi\mu\mathbf{u}(\mathbf{x}) = \int_D \frac{(r^2 + 2\epsilon^2)\mathbf{f}(s) + (\mathbf{f}(s)\cdot\mathbf{r})\mathbf{r}}{(r^2+\epsilon^2)^{3/2}} ds \tag{2.8}$$

where $\mathbf{r} = \mathbf{x} - \mathbf{x}(s)$, $r = \|\mathbf{r}\|$, and D is the surface of the helical ring. The regularization parameter ϵ is typically chosen on the order of the surface discretization.

2.2. *Dynamic, elastic calculations*

Dynamic simulations of the helical ring can be computed through the use of an elasticity model that provides the forces on the flagellum from its current geometry, and using those forces to compute the surface velocity through Eq. (2.4). We discretize the surface of the helical tube with points along circular cross-sections. Each point is connected by springs to several other nearby points. Each spring is assigned a stiffness constant κ_{Sj}

and a resting length δ_j. The simulation is accomplished by dynamically changing the resting lengths of all springs in order to induce a traveling wave along the helix.

Assume that at time $t = t_n$ we know the location of all surface points $\mathbf{x}_k$ ($k = 1, 2, \ldots, N_p$) and the resting lengths $\delta_j(t_n)$ ($j = 1, 2, \ldots, N_s$) of all springs. The computation proceeds as follows:

(a) For $k = 1, 2, \ldots, N_p$, compute the force $\mathbf{f}_k$ at $\mathbf{x}_k$ by

$$\mathbf{f}_k = \sum_j \frac{\kappa_{Sj}}{\delta_j(t_n)} \left(\|\mathbf{x}_k - \mathbf{x}_{k(j)}\| - \delta_j(t_n) \right) \frac{\mathbf{x}_{k(j)} - \mathbf{x}_k}{\|\mathbf{x}_k - \mathbf{x}_{k(j)}\|}$$

where the sum is over all springs that connect $\mathbf{x}_k$ to other points $\mathbf{x}_{k(j)}$.

(b) Given the forces $\mathbf{f}_k$, use a discretization of Eq. (2.8) to compute the velocities $\mathbf{u}(\mathbf{x}_k)$ and evolve the particles by $d\mathbf{x}_k/dt = \mathbf{u}(\mathbf{x}_k)$ one time step.

We note that since all forces are derived from springs, the net force and net torque are automatically zero. The spring stiffnesses must be adjusted so that the structure remains approximately inextensible. In all computations, we set all spring stiffnesses to 1.

3. Numerical results

3.1. *Model problem*

We begin our investigation of the fluid dynamics of waving cylindrical rings by choosing one with three pitches $p = 3$ around a circle of dimensionless radius $r = 0.5$, amplitude $R = 0.09$, with a traveling wave of temporal period $T = 20\pi$ ($\omega = 0.1$) (see Eq. (2.1)). The cross sectional radius of the tube is $r_h = 0.035$. Figure 2 shows instantaneous streamlines induced by the waving cylindrical ring, upon which a traveling wave tangential to the ring is imposed. This wave moves counterclockwise when viewed from above. Note that there is significant upwards flow in the center of the ring that results from the rotational flow supported by each of the circular cross-sections of the ring. Figure 3 shows snapshots

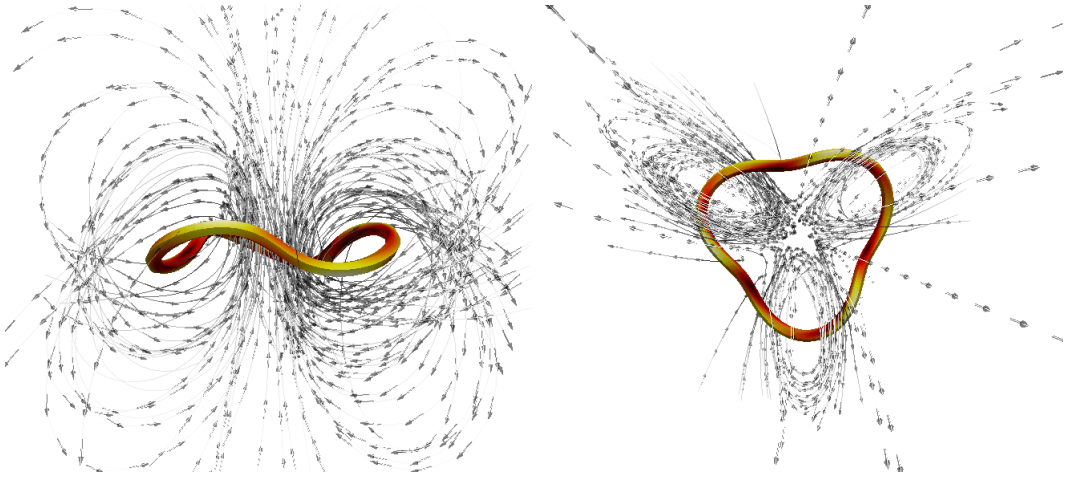

FIGURE 2. Instantaneous three-dimensional streamlines induced by the waving cylindrical ring from different perspectives. The traveling wave is counterclockwise when viewed from above.

of the ring as the wave progresses within a period, along with velocity fields projected onto the xz-plane (top) and the xy-plane (bottom). Although the ring is periodic, we place a cut in it to demonstrate that there is tangential motion of material points of the ring in the direction opposite of the wave. Even though these snapshots depict a very short time interval, one can also note a slight shift upwards of the ring in the xy-plane as the wave progresses.

The velocity fields shown in Figures 2 and 3 were computed using the dynamic regularized Stokeslet formulation. The ring was discretized using 110 circular cross sections, with 6 points on each cross sections (N_p=660). The regularization parameter was chosen to coincide roughly with the average distance between points that discretize the surface of the ring (Cortez *et al.* (2005)).

3.2. *Effect of wave amplitude on velocities*

Here we examine the effect of wave amplitude R on the rotational and translational velocities of the ring. We define the rotational velocity to be the velocity tangential to the circular axis of the ring's helical centerline, and denote this velocity by VT. Similarly, we define the translational velocity to be the velocity perpendicular to the plane of this

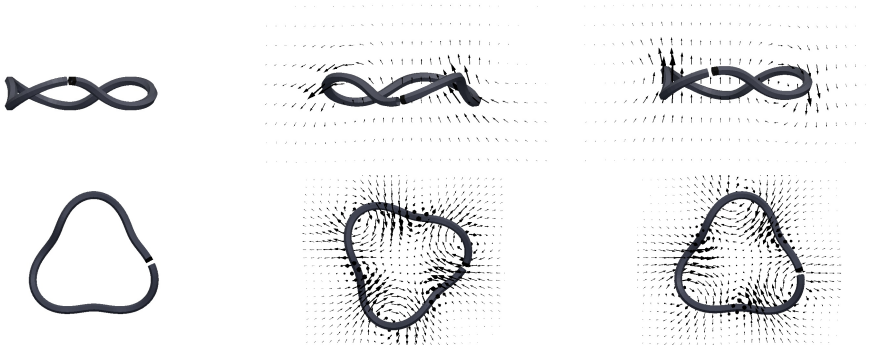

FIGURE 3. Snapshots within one period of ring and velocity fields on the xz-plane (top) and xy-plane (bottom) of a waving cylindrical ring with three pitches. Time increases from left to right. Note that the a cut on the ring is included to depict tangential motion.

circular axis, and denote this velocity by VB. We remind the reader that the classical analysis of Taylor (1952) showed that, for small amplitude R, a waving cylindrical ring whose axis was straight gave rise to velocities $VT = O(R^2)$ in the direction tangential to the axis. Of course, the order must be even in the amplitude, since the geometry is unchanged when R is replaced by $-R$. Using the same geometric parameters as in the model problem above, we use slender body theory, instantaneous regularized Stokeslet calculations, and a dynamic Stokeslet simulation to compute VT and VB for different amplitudes R. Figure 4 shows a log-log plot of normalized velocities versus normalized helix amplitude. Here, we scale each velocity by the imposed wavespeed, and the amplitude of the helical wave is scaled by the wavelength. We also plot $(R/\lambda)^2$ for reference. We see that both the rotational and translational velocity exhibit $O(R^2)$ behavior, with some deviation in the rotational velocity for larger amplitudes R. In comparing the numerical approaches, we see that the calculated VT and VB using the steady Stokeslet or dynamic Stokeslet formulations are indistinguishable. Both Stokeslet formulations discretize the surface of the cylindrical tube, while slender body theory relies only on a discretization of the helical centerline. While slender body theory slightly overestimates the rotational velocity, it captures translational velocities that are also indistinguishable from the Stokeslet formulations. Note that our Stokeslet formulations used a surface dis-

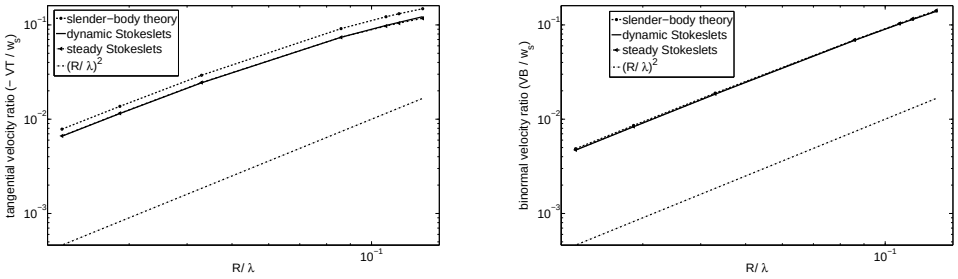

FIGURE 4. Log-log plots of (left) $-VT/w_s$ versus R/λ and (right) VB/w_s versus R/λ computed using slender body theory, instantaneous (static) regularized Stokeslets, and dynamic regularized Stokeslets.

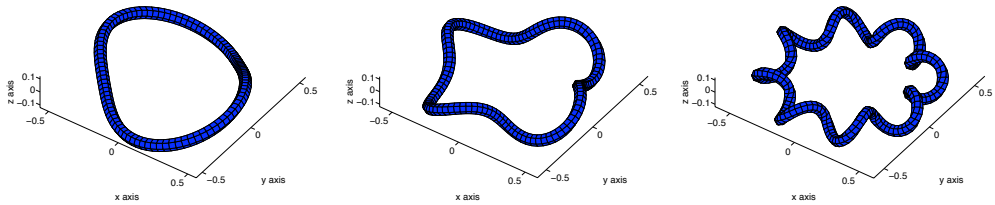

FIGURE 5. Cylindrical ring with 2,4, and 8 pitches

.

cretization as described above, and our slender body calculations discretize the centerline using 2500 points, with integrals approximated by the trapezoidal rule. In the dynamic simulations, the velocities reported were computed after a short transient time interval.

3.3. *Effect of number of pitches around ring on velocities*

We examine the effect of varying the number of pitches on a cylindrical ring, with all other geometric parameters fixed (see Figure 5 for examples of these geometries). Note that a cylindrical tube with zero pitches around the circle is just a closed torus, and no traveling wave can be imposed. Moreover, since the tube has finite diameter, there is a maximal number of pitches that can actually be realized. As the number of pitches reaches this maximal values, the profile that the ring presents to the fluid would be nearly that of a torus again, and the propulsion would be inefficient. We expect, therefore, that there will be an optimal number of pitches for a given geometry of the ring that will maximize rotational velocity VT. (This property was also observed for a straight helix in

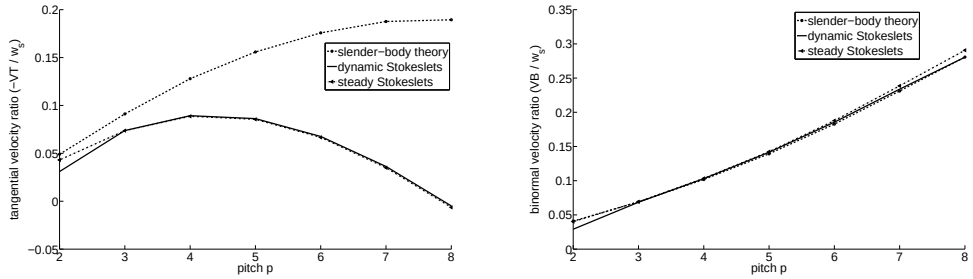

FIGURE 6. (left) $-VT/w_s$ versus number of pitches p and (right) VB/w_s versus number of pitches p computed using slender body theory, instantaneous regularized Stokeslets, and dynamic Stokeslet simulations.

Cortez *et al.* (2005).) However, as will be discussed below, each cross section of the tube in this extreme case is still undergoing a periodic orbit reminiscent of Purcell's toroidal swimmer (Leshansky & Kenneth (2008)) that will result in translational motion. Figure 6 shows plots of the normalized velocities $-VT/w_s$ and VB/w_s versus number of pitches p computed using slender body theory, instantaneous regularized Stokeslets, and dynamic Stokeslet simulations. We see that both Stokeslet formulations capture the existence of an optimum pitch for maximizing rotational velocity VT, but the slender body theory does not. We also see that the translational velocities increase with the number of pitches, and that there is excellent agreement among all three numerical methods in the computation of VB.

3.4. *Effect of radius of baseline circle on velocities*

Here we examine how rotational and translational velocities change as the baseline circle increases in diameter (see Figure 7 for examples of these geometries). The periodic cylindrical tail analyzed in Taylor (1952) swims opposite the direction of the traveling wave, and by no means exhibits any swimming normal to that direction. The translational velocity of the cylindrical ring, however, arises precisely because of its circular shape and the collective stirring by cross sections of the ring. As the radius of the baseline circle increases, we expect the translational velocity to decrease, and the rotational velocity to

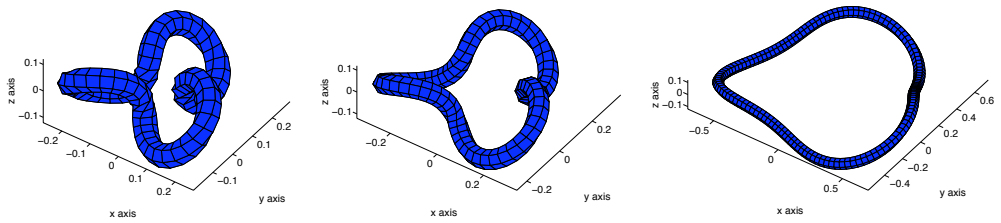

FIGURE 7. Cylindrical rings with all geometric parameters fixed as in the model problem, except for radius of baseline circle. Shown here are the cases $r = \frac{1}{6}$, $r = \frac{1}{4}$, and $r = \frac{5}{8}$. Note that the scales of the axis are different in the different plots.

converge to the swimming velocity of a straight, infinite helix. This behavior is, indeed, reflected in the calculations presented in Figure 8, which shows $-VT/w_s$ and VB/w_s versus r computed using slender body theory, instantaneous regularized Stokeslets, and dynamic Stokeslet simulations. Moreover, we see that for the smallest baseline radius, regularized Stokeslet formulations show that the rotational velocity of the ring is in the same direction of the wave! The first frame in Figure 7 demonstrates the complexity of the geometry of this case, and gives a visual indication that the assumptions of slender body theory are not appropriate. However, we see that as the baseline circle increases in diameter, the rotational velocities computed using slender body theory approach those arrived at by the Stokeslet formulations.

We remark that we could non-dimensionalize Eq. (2.1) by choosing the length scale $\ell = r$ and velocity scale $U = \omega\lambda/2\pi$, giving us a non-dimension amplitude $R^* = R/r$ and a non-dimensional tube radius $r_h^* = r_h/r$. Here, however, we chose to vary the radius of the baseline circle while keeping the tube radius r_h fixed. As can be seen in frames of Figure 7 where the scales of the axes change with r, the non-dimensional amplitude decreases with increasing r, as does the slenderness r_h/L of the flagellum. Therefore, for large values of r, the flagellum has smaller amplitude and is more slender, meeting more closely the assumptions of slender-body theory.

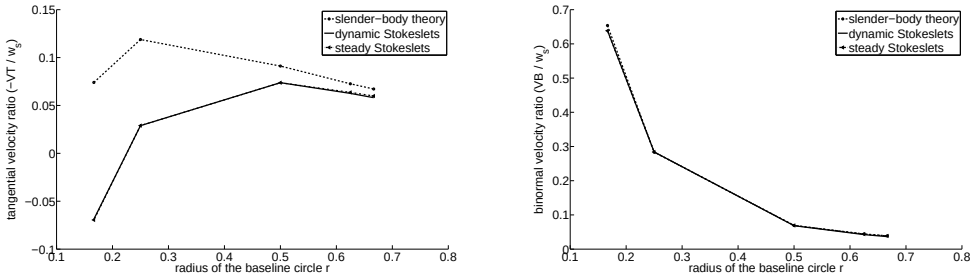

FIGURE 8. (left)$-VT/w_s$ versus r and (right)VB/w_s versus r computed using slender body theory, instantaneous regularized Stokeslets, and dynamic Stokeslet simulations. Here r is the radius of the baseline circle.

3.5. *Comparison with toroidal swimmer*

In both Taylor (1952) and Purcell (1977), a drawing of a hypothetical simple swimmer in the shape of a cylinder wrapped into a torus was presented. Would the twirling of each of the circular cross sections about the circular torus axis, at constant angular velocity, cause the torus to swim in a Stokes fluid? Recently, Leshansky & Kenneth (2008) analyzed this toroidal swimming due to surface rotations, and showed that the swimmer is propelled against the direction of its outer surface. For the ratio $s_0 = b/a$, where b is the radius of the circular axis of the torus, a is the cross-section radius, and u_s the angular velocity of each cross section, they compute a translational velocity $V \approx \frac{u_s}{2s_0}(\log 8s_0 - \frac{1}{2})$ in the limit of large s_0. Figure 9 allows us to visualize the relationship between our waving cylindrical ring and the toroidal swimmer, by inscribing the cylindrical ring in a torus whose radius is $b = r$ and whose cross-sectional radius is $a = R + r_h$. For the torus, each point on a circular cross section is rotating with a constant angular velocity. On the other hand, only a segment of the helical tube, while tracing out roughly the same cross section of the circumscribing torus, contributes an angular velocity. Figure 9 shows the comparison of the computed scaled translational velocity versus the ratio s_0 for the helical ring, along with the asymptotic results for the circumscribing torus in Leshansky & Kenneth (2008). As expected, the translational velocity of the torus is greater than

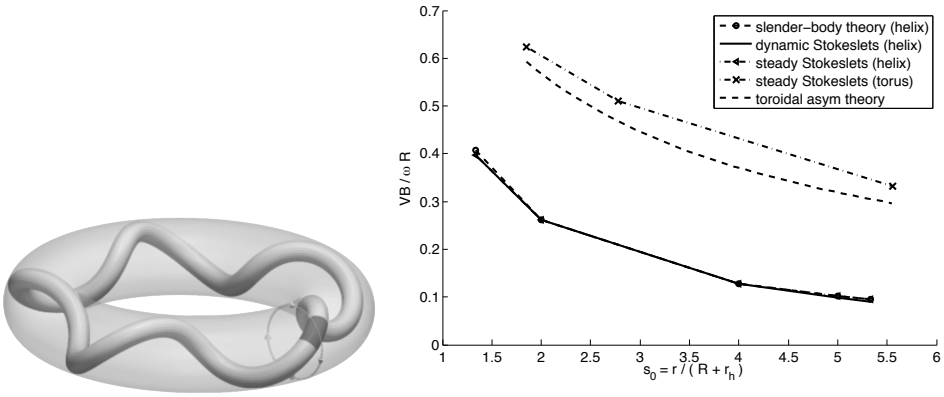

FIGURE 9. (left) Visualization of the helical tube inscribed in a torus. (right) $VB/\omega R$ versus s_0 computed for the helical ring. In addition, the scaled translational velocities for the circumscribing torus predicted by the asymptotic theory from Leshansky & Kenneth (2008) are shown, along with regularized Stokeslet computations of these toroidal swimming velocities.

that of the inscribed helical ring. In addition, we computed the translational velocity of the toroidal swimmer using steady Stokeslet calculations, and these values show good agreement with the asymptotic theory (see Figure 9).

4. Discussion

In an effort to understand the function of the longitudinal flagellum of dinoflagellates, we have formulated a simple fluid mechanical system of a waving cylindrical ring moving in a Stokes fluid. We conclude that the traveling wave imposed around the ring induces both rotational and translational motion. We have also used this model system to compare regularized Stokeslet formulations to slender body theory, two popular numerical methods for Stokes flow. When computing rotational velocities of the ring, slender body theory calculations agree very well with regularized Stokeslet calculations for baseline circles of large radii and rings supporting smaller numbers of helical pitches. In these cases, the assumptions of slender body theory are more closely met. What is striking is the consistent, close agreement between the two numerical approaches when computing translational velocities. We conjecture that the largest contribution to the rotational ve-

locity at a cross-section comes from the cross-section itself and others nearby. It is a local process. On the other hand, the translational velocity at a cross-section is a result of the far field flow generated by the portion on the opposite side of the tube. We conclude that the translational velocity is less sensitive to local changes in the geometry than the rotational velocity, allowing slender body approximations to still give good approximations. We remark that we have chosen not to compute velocities based upon resistive force theory, since it has been shown to give significant errors for helical filaments with appreciable curvature (Yand *et al.* (2009); Jung *et al.* (2007)).

Recently, the method of Regularized Stokeslets has been used as a computational framework for modeling low Reynolds number flows around cilia and flagella (e.g. Gillies *et al.* (2009); Qian *et al.* (2009); Smith (2009)). In the majority of these applications, the flow is induced by prescribing the kinematics of the immersed structure. However, the regularized Stokeslet formulation easily captures the coupling of flexible structure with the surrounding fluid (e.g. Flores *et al.* (2005)). In this case, forces due to passive elasticity and active bending moments applied by the immersed structure induce the flow, and the geometry of the structure emerges from the resulting velocity. Here, we have solved the helical ring problem by prescribing kinematics as well as by using an elastic model that achieves the desired kinematics by specifying time-dependent rest lengths of stiff springs connecting points on the surface of the ring. We believe that the simple model problem presented here provides a validation in support of other dynamic Stokeslet models.

While we have now achieved an understanding of the motion of an isolated waving cylindrical ring, more work remains in analyzing the fluid dynamics of dinoflagellate swimming. Future models will include the presence of a cell body and a longitudinal flagellum, along with the study of fluid-dynamic interactions between model dinoflagellates.

Acknowledgements: The work of H. Nguyen and L. Fauci was partially funded by NSF

grant NSF-OCE 0724598. The work of R. Ortiz and R. Cortez was partially funded by NSF grants DMS-0612625 and EPS-0701491.

REFERENCES

Cachon, M., Cachon, J., Cosson, J., Greuet, C. & Huitorel, P. 1991 Dinoflagellate flagella adopt various conformations in response to different needs. *Biol. Cell* **71**, 175–182.

Cortez, R. 2001 The method of regularized Stokeslets. *SIAM J. Sci. Comput.* **23**, 1204.

Cortez, R., Fauci, L. & Medovikov, A. 2005 The method of regularized Stokeslets in three dimensions: analysis, validation, and application to helical swimming. *Phys. Fluids* **17**, 031504.

Fenchel, T. 2001 How dinoflagellates swim. *Protist* **152**, 329–338.

Flores, H., Lobaton, E., Mendez-Diez, S., Tlupova, S. & Cortez, R. 2005 A study of bacterial flagellar bundling. *Bull. Math. Bio.* **67**, 137–168.

Gaines, G. & Taylor, F. 1985 Form and function of the dinoflagellate transverse flagellum. *J. Protozool.* **32** (2), 290–296.

Gillies, E., Cannon, R., Green, R. & Pacey, A. 2009 Hydrodynamic propulsion of human sperm. *J. Fluid Mech.* **625**, 445–474.

Jung, S., Mareck, K., Fauci, L. & Shelley, M. 2007 Rotational dynamics of a superhelix towed in a Stokes fluid. *Phys. of Fluids* **19**, 103105.

Latz, M., Bovard, M., VanDelinder, V., Segre, E., Rohr, J. & Groisman, A. 2008 Bioluminescent response of individual dinoflagellate cells to hydrodynamic stress measured with millesecond resolution in a microfluidic device. *J. Exp. Biol.* **211**, 2865–2875.

Leshansky, A. & Kenneth, O. 2008 Surface tank treading: Propulsion of Purcell's toroidal swimmer. *Phys. Fluids* **20**, 063104.

Lighthill, JL 1976 Flagellar hydrodynamics. *SIAM Review* **18**, 161.

Miyasaka, I., Nanba, K., Furuya, K., Nimura, Y. & Azuma, A. 2004 Functional roles of the transverse and longitudinal flagella in the swimming motility of *prorocentrum minimum* (dinophyceae). *J. Exp. Biol.* **207**, 3055–3066.

Purcell, E.M. 1977 Life at low Reynolds numbers. *Am. J. Phys.* **45**, 3–11.

Qian, B., Jiang, H., Gagnon, D., Breuer, K. & Powers, T. 2009 Minimal model for synchronization induced by hydrodynamic interactions. *Phys. Rev. E* **80**, 061919.

Sheng, J., Malkiel, E., Katz, J., Adolf, J., Belas, R. & Place, A. 2007 Digital holographic microscopy reveals prey-induced changes in swimming behavior of predatory dinoflagellates. *Proc. Natl. Acad. Sci.* **104** (44), 17512–17517.

Smith, D.J. 2009 A boundary element regularized Stokeslet method applied to cilia-and flagella-driven flow. *Proc. R. Soc. A.* **465**, 3605–3626.

Taylor, G. I. 1952 The action of waving cylindrical tails in propelling microscopic organisms. *Proc. R. Soc. A* **211**, 225–239.

Yand, J., Wolgemuth, C. & Huber, G. 2009 Kinematics of thte swimming of *spiroplasma*. *Phys. Rev. Letters* **102**, 218102.